Vlasov-Poisson Simulation of Self-Gravitating Systems and Its Application to Cosmological Neutrinos in the Large-Scale Structure in the Universe

Kohji Yoshikawa

Center for Computational Sciences, University of Tsukuba

"Collisionless Boltzmann (Vlasov) Equation and Modeling of Self-Gravitating Systems and Plasmas"
October 30 - November 3, 2017, CIRM, Marseille, France

collaborators: Satoshi Tanaka (CCS, Univ. of Tsukuba)
Takashi Minoshima (JAMSTEC)
Naoki Yoshida (Univ. of Tokyo)

Contents

N-body Simulation

- a standard method for simulations of self-gravitating systems (galaxies, clusters of galaxies, the LSS) for more than 40 years.

- the mass distribution is sampled by particles in the 6D phase-space volume (**x**, **p**) in a Monte-Carlo manner.

⇨ need for a very large number of particles

$$\frac{\mathrm{d}\boldsymbol{v}_i}{\mathrm{d}t} = \sum_j \frac{m_j(\boldsymbol{r}_j - \boldsymbol{r}_i)}{|\boldsymbol{r}_j - \boldsymbol{r}_i|^3}$$

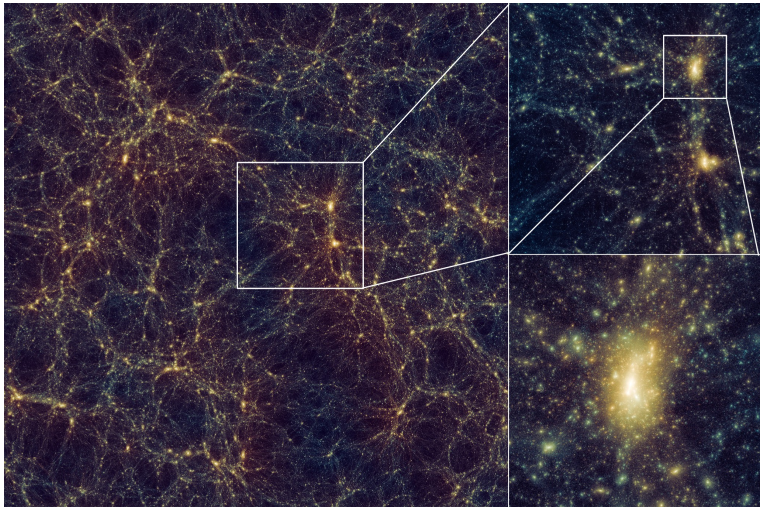

Ishiyama

- sophisticated algorithms to treat large number of particles such as Tree and TreePM methods developed

Particle-In-Cell (PIC) Simulation

- Particle-based approach to solve collisionless (astrophysical) plasma

$$\frac{\mathrm{d}\boldsymbol{v}_i}{\mathrm{d}t} = \frac{q_i}{m_i}\left(\boldsymbol{E} + \frac{\boldsymbol{v}_i \times \boldsymbol{B}}{c}\right)$$

- E- and B-field are computed in the finite difference manner

$$\boldsymbol{x}_i, \boldsymbol{v}_i \Rightarrow \boldsymbol{J}$$

$$\frac{\partial \boldsymbol{E}}{\partial t} = c\nabla \times \boldsymbol{B} - 4\pi \boldsymbol{J}$$

$$\frac{\partial \boldsymbol{B}}{\partial t} = -c\nabla \times \boldsymbol{E}$$

- particle acceleration in collisionless shock
- magnetic reconnection

3D PIC simulation of collisionless shock

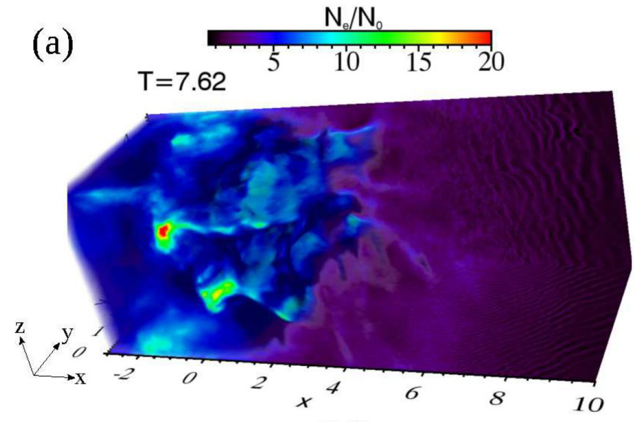

Matsumoto et al. (2017)

PIC simulation of magnetic reconnection

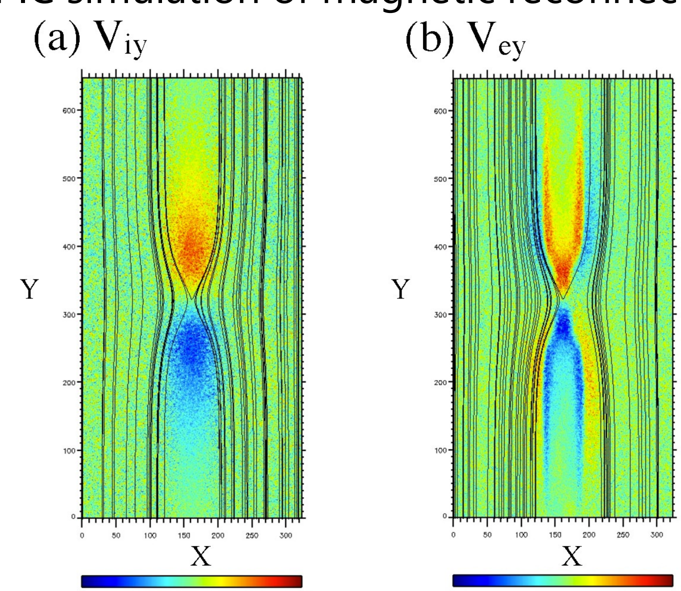

(pCANS web page)

Drawbacks of Particle Simulations

- intrinsic contamination of shot noise in physical quantities
  - "sheet in phase space" approach can reduce such noise in the cold limit. (Shandarin et al. 2012, Abel et al. 2012, Oliver et al. 2013)

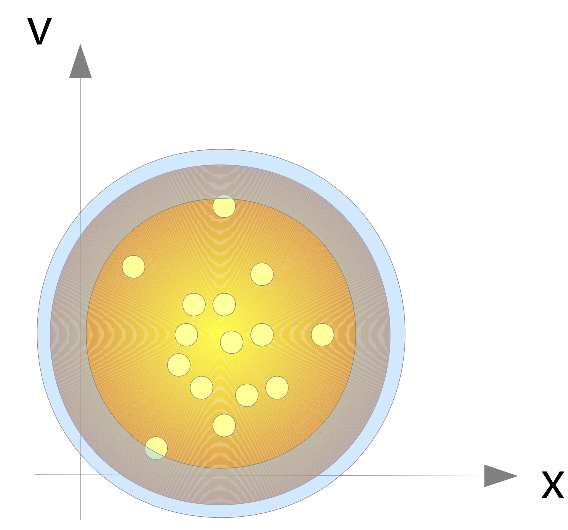

- not good at simulating kinetic physical processes in which the tail of the distribution function plays important roles
  - matter in the tail is not fairly sampled in particle simulations
  - collisionless damping, two-stream instability
  - magneto-rotational instability starting from high-beta plasmas

- The grid spacing of PIC simulation should be less than the Debye length.
  - difficult to simulate phenomena in the macroscopic MHD scale

Vlasov Simulations

- Directly solving the Vlasov equation

$$\frac{\partial f}{\partial t} + \frac{\mathrm{d}\boldsymbol{x}}{\mathrm{d}t} \cdot \frac{\partial f}{\partial \boldsymbol{x}} + \frac{\mathrm{d}\boldsymbol{p}}{\mathrm{d}t} \cdot \frac{\partial f}{\partial \boldsymbol{p}} = 0$$

- Vlasov-Poisson simulation
  - self-gravitating system
  - electro-static plasma

$$\frac{\partial f}{\partial t} + \boldsymbol{v} \cdot \frac{\partial f}{\partial \boldsymbol{x}} - \nabla\phi \cdot \frac{\partial f}{\partial \boldsymbol{p}} = 0$$

$$\nabla^2\phi = 4\pi G\rho = 4\pi G \int f \mathrm{d}^3\boldsymbol{v}$$

- Vlasov-Maxwell simulation
  - magnetized plasma

$$\frac{\partial f_\mathrm{s}}{\partial t} + \boldsymbol{v} \cdot \frac{\partial f_\mathrm{s}}{\partial \boldsymbol{x}} + \frac{q_\mathrm{s}}{m_\mathrm{s}} \left(\boldsymbol{E} + \frac{\boldsymbol{v} \times \boldsymbol{B}}{c} \right) \cdot \frac{\partial f_\mathrm{s}}{\partial \boldsymbol{v}} = 0$$

$$\frac{\partial \boldsymbol{E}}{\partial t} = c\nabla \times \boldsymbol{B} - 4\pi \boldsymbol{J}$$

$$\frac{\partial \boldsymbol{B}}{\partial t} = -c\nabla \times \boldsymbol{E}$$

$$\boldsymbol{J} = \sum_\mathrm{s} \int q_\mathrm{s} \boldsymbol{v} f_\mathrm{s} \mathrm{d}^3\boldsymbol{v}$$

Vlasov-Poisson Simuation in 6D phase space

Yoshikawa, Yoshida, Umemura (2013)

- directional splitting method

$$\frac{\partial f}{\partial t} + \vec{v} \cdot \frac{\partial f}{\partial \vec{x}} - \nabla \phi \cdot \frac{\partial f}{\partial \vec{v}} = 0 \quad \Rightarrow \quad \begin{cases} \dfrac{\partial f}{\partial t} + v_i \dfrac{\partial f}{\partial x_i} = 0 & (i = 1, 2, 3) \\[2ex] \dfrac{\partial f}{\partial t} - \dfrac{\partial \phi}{\partial x_i} \dfrac{\partial f}{\partial v_i} = 0 & (i = 1, 2, 3) \end{cases}$$

$$\begin{aligned} f(\vec{x}, \vec{v}, t^{n+1}) = {} & T_{v_x}(\Delta t/2) T_{v_y}(\Delta t/2) T_{v_z}(\Delta t/2) \\ & T_x(\Delta t) T_y(\Delta t) T_z(\Delta t) \\ & T_{v_x}(\Delta t/2) T_{v_y}(\Delta t/2) T_{v_z}(\Delta t/2) \quad f(\vec{x}, \vec{v}, t^n) \end{aligned}$$

$T_\ell(\Delta t)$: advection along ℓ-direction

- numerical scheme for a one-dimensional advection equation

Positive and Flux Conservative (PFC) scheme   Filbet, Sonnendrücker, Bertrand (2001)

Merging of Two King Spheres

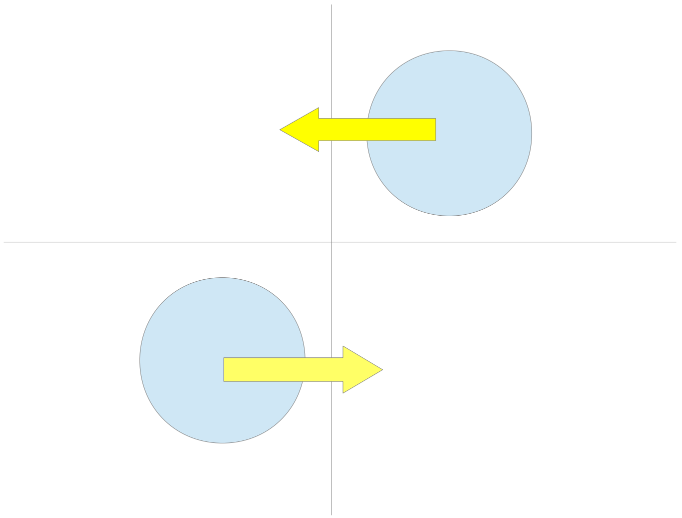

- offset merging of two king spheres
- comparison with a equivalent N-body simulations, in which each King sphere is represented with a million particles

Vlasov simulation

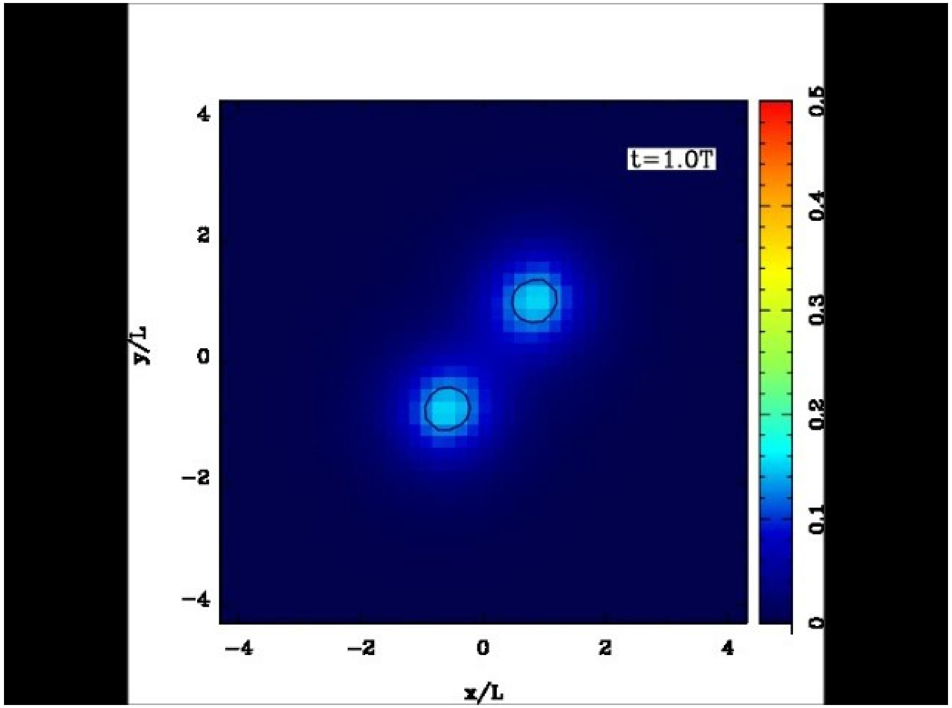

N-body simulation

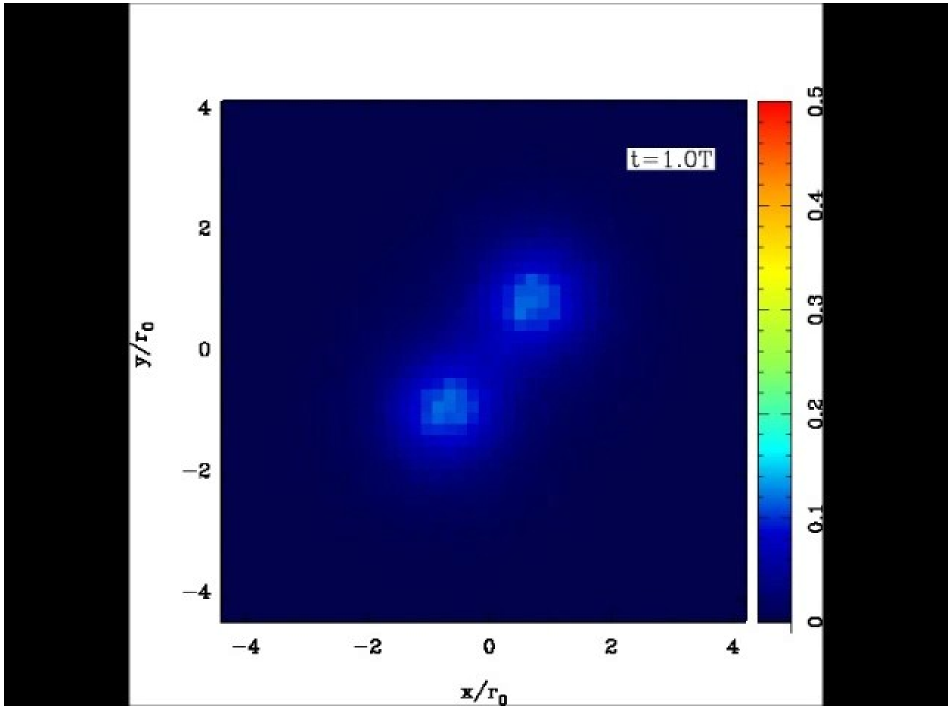

Grav. Instablity and Collisionless Damping

Initial condition

$$\begin{cases} f(\vec{x},\vec{v},t=0) = \dfrac{\bar{\rho}(1+\delta(x))}{(2\pi\sigma^2)^{3/2}} \exp\left(-\dfrac{|\vec{v}|}{2\sigma^2}\right) \\ \rho(x,t=0) = \bar{\rho}(1+\delta(x)) \end{cases}$$

$k < k_\mathrm{J}$: gravitational instability

$k > k_\mathrm{J}$: collisionless damping

- The density fluctuation *δ (x)* is given so that it has a white noise power spectrum.

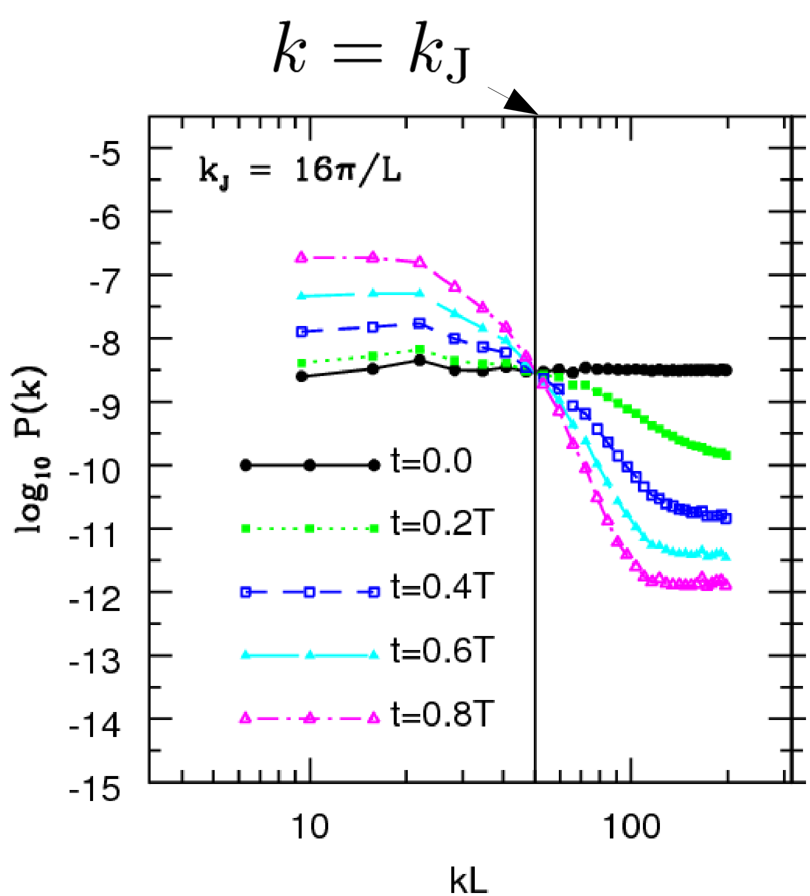

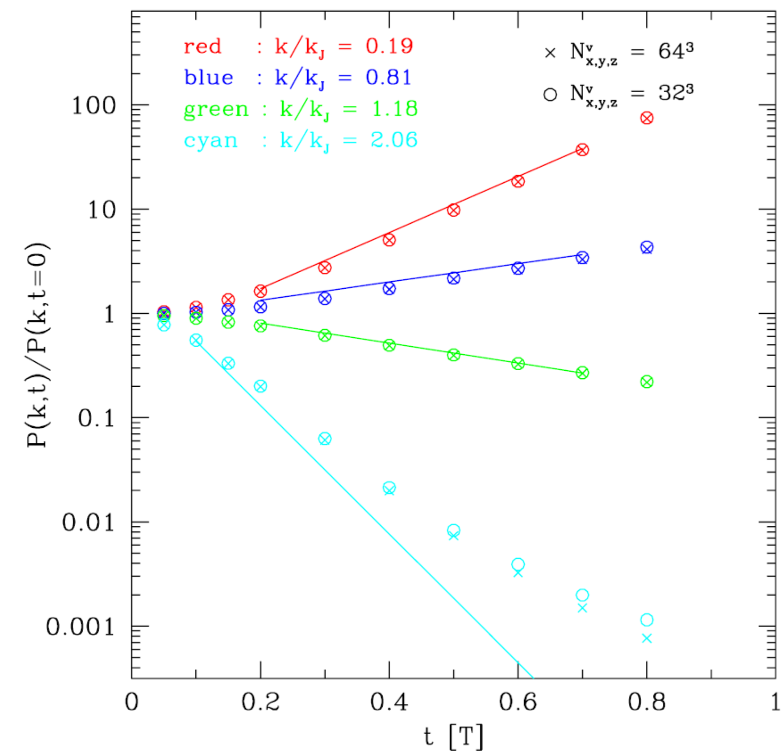

lines : theoretical prediction

New High-Order Scheme for Vlasov Simulation

Higher-Order Advection Schemes

- curse of dimensionality in Vlasov simulations

  huge memory consumption due to high dimensionality of phase space

  ⇨ size of numerical simulation is limited by the amount of available memory

- how to overcome
  - adaptive mesh refinement (Deriaz et al 2015)
  - higher-order scheme for advection equation

$$\frac{\partial f(x,t)}{\partial t} + c\frac{\partial f(x,t)}{\partial x} = 0$$

- spatially fifth- and seventh-order schemes with monotonicity- and positivity-preserving features.

  (c.f. The PFC scheme has a spatially third-order accuracy.)

- mathematical and physical requirement
  - monotonicity
  - positivity
  - maximum principle

Monotonicity and Positivity

$$\frac{\partial f(x,t)}{\partial t} + c\frac{\partial f(x,t)}{\partial x} = 0 \quad \Rightarrow \quad f_i^{n+1} = f_i^n - \frac{\Delta t}{\Delta x}(F_{i+1/2}^n - F_{i-1/2}^n)$$

numerical flux : $F_{i+1/2}^n = c f_{i+1/2}^n$

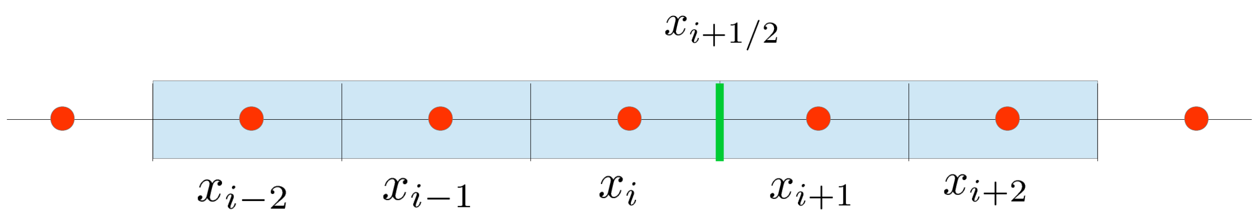

- 5th-order interpolation of the boundary value

$$f_{i+1/2}^{\mathrm{int}} = (2f_{i-2} - 13f_{i-1} + 47f_i + 27f_{i+1} - 3f_{i+2})/60$$

- Higher-order interpolation usually violates the monotonicity after Godunov's theorem

- constraints to preserve the mononicity of numerical solutions

$$\boxed{f_{i+1/2}^{\mathrm{MP}} = \mathrm{MP}(f_{i+1/2}^{\mathrm{int}}, f_{i-2}, f_{i-1}, f_i, f_{i+1}, f_{i+2})}$$

MP for monotonicity preservation

Positivity Preserving Limiter

- positivity of numerical solutions

$$\forall i \qquad f_i^n \geq 0 \Longrightarrow f_i^{n+1} \geq 0$$

- monotonicity does not assure positivity

- positivity preserving boundary values can be computed in a flux limiter manner

$$\hat{f}_{i+1/2} = \theta_{i+1/2} \underline{f^{\mathrm{MP}}_{i+1/2}} + (1 - \theta_{i+1/2}) \underline{f^{\mathrm{UP}}_{i+1/2}}$$

monotonocity preserving boundary value

boundary value for the first-order upwind scheme

- By setting a parameter $\theta_{i+1/2}(f_i, f_{i+1})$ properly, we can construct the boundary value for the monotonicity- and positivity-preserving (MPP) scheme

$$\boxed{\hat{f}_{i+1/2} = \mathrm{PP}(f^{\mathrm{MP}}_{i+1/2}, f_i, f_{i+1})}$$

TVD Runge-Kutta Time Integration

- Accuracy of Time Integration
  - A spatially higher-order scheme needs higher-order time integration schemes
  - Spatially fifth-order MPP5 scheme needs temporaly third-order scheme

3-stage 3rd-order TVD-Runge-Kutta scheme

$$\begin{cases} f_i^{(1)} = f_i^n - \nu L_i(f^n) \\ f_i^{(2)} = \dfrac{3}{4} f_i^n + \dfrac{1}{4}\left(f_i^{(1)} - \nu L_i(f^{(1)})\right) \\ f_i^{n+1} = \dfrac{1}{3} f_i^n + \dfrac{2}{3}\left(f_i^{(2)} - \nu L_i(f^{(2)})\right) \end{cases} \Rightarrow \text{RK-MPP5 scheme}$$

  - Spatially higher-order scheme (e.g. MPP7 or MPP9) needs temporaly even higher-order scheme.

    4-stage 4th-order TVD-RK scheme for MPP7

    6-stage 6th-order TVD-RK scheme for MPP9

computationally too expensive!!

Semi-Lagrange Time Integration

- Conservative Semi-Lagrange scheme

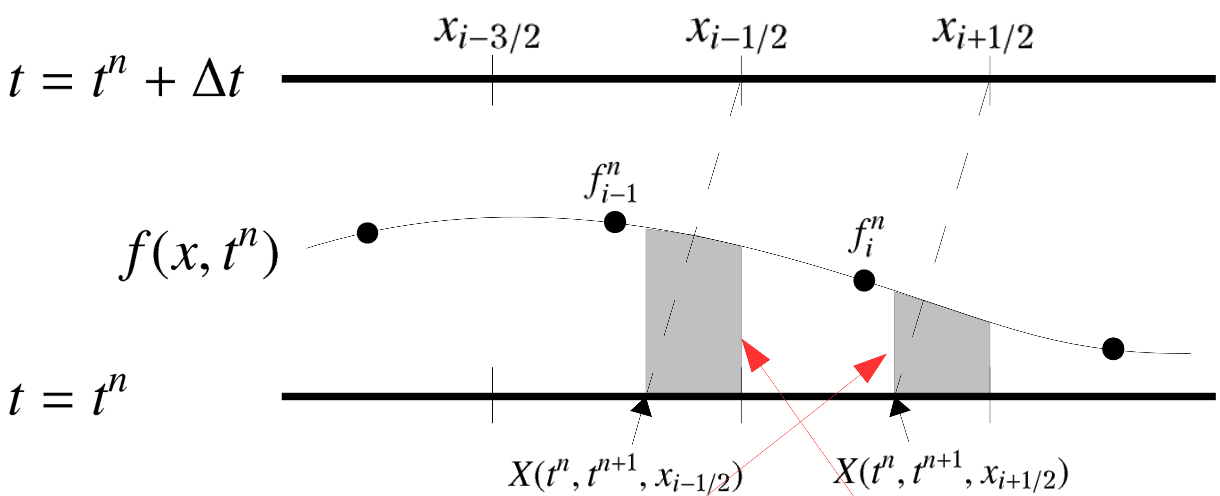

$$f_i^{n+1} = f_i^n - \nu\left(\boxed{\Phi_{i+1/2}^n} - \boxed{\Phi_{i-1/2}^n}\right)$$

- boundary values of spatially fifth-order conservative SL scheme

$$\Phi_{i-1/2}^n = \sum_{j=0}^{4} C_j \zeta^j \qquad \zeta = \frac{c\Delta t}{\Delta x}$$

$$C_0 = \frac{f_{i-3}^n}{30} - \frac{13}{60}f_{i-2}^n + \frac{47}{60}f_{i-1}^n + \frac{9}{20}f_i^n - \frac{f_{i+1}^n}{20}$$

$$C_1 = -\frac{f_{i-2}^n}{24} + \frac{5}{8}f_{i-1}^n - \frac{5}{8}f_i^n + \frac{f_{i+1}^n}{24}$$

$$C_2 = -\frac{f_{i-3}^n}{24} + \frac{f_{i-2}^n}{4} - \frac{f_{i-1}^n}{3} + \frac{f_i^n}{12} + \frac{f_{i+1}^n}{24}$$

$$C_3 = \frac{f_{i-2}^n}{24} - \frac{f_{i-1}^n}{8} + \frac{f_i^n}{8} - \frac{f_{i+1}^n}{24}$$

$$C_4 = \frac{f_{i-3}^n}{120} - \frac{f_{i-2}^n}{30} + \frac{f_{i-1}^n}{20} - \frac{f_i^n}{30} + \frac{f_{i+1}^n}{120}$$

Qiu, J.-M., Christlieb, A., 2010, JCP, 229, 1130-1149

Semi-Lagrange Schemes

- boundary values with conservative SL schemes do not preserve the monotonicity and the positivity of numerical solutions.

- monotonicity-preserving schemes by applying MP constraints to $\Phi_{i+1/2}$

$$\Phi^{\mathrm{MP},n}_{i+1/2} = \mathrm{MP}(\Phi^n_{i+1/2}, f^n_{i-2}, f^n_{i-1}, f^n_i, f^n_{i+1}, f^n_{i+2})$$

SL-MP5 / SL-MP7 scheme : $f_i^{n+1} = f_i^n - \nu(\Phi^{\mathrm{MP},n}_{i+1/2} - \Phi^{\mathrm{MP},n}_{i-1/2})$

- monotonicity- and positivity-preserving schemes by futher applying PP limiter

$$\hat{\Phi}^n_{i+1/2} = \mathrm{PP}(\Phi^{\mathrm{MP},n}_{i+1/2}, f^n_i, f^n_{i+1})$$

SL-MPP5 / SL-MPP7 scheme : $f_i^{n+1} = f_i^n - \nu(\hat{\Phi}^n_{i+1/2} - \hat{\Phi}^n_{i-1/2})$

- These schemes perform single-stage time integration irrespetive of the spatial order of accuracy

Linear Advection

- linear advection of $f(x, t=0) = \sin^4(4\pi x)$

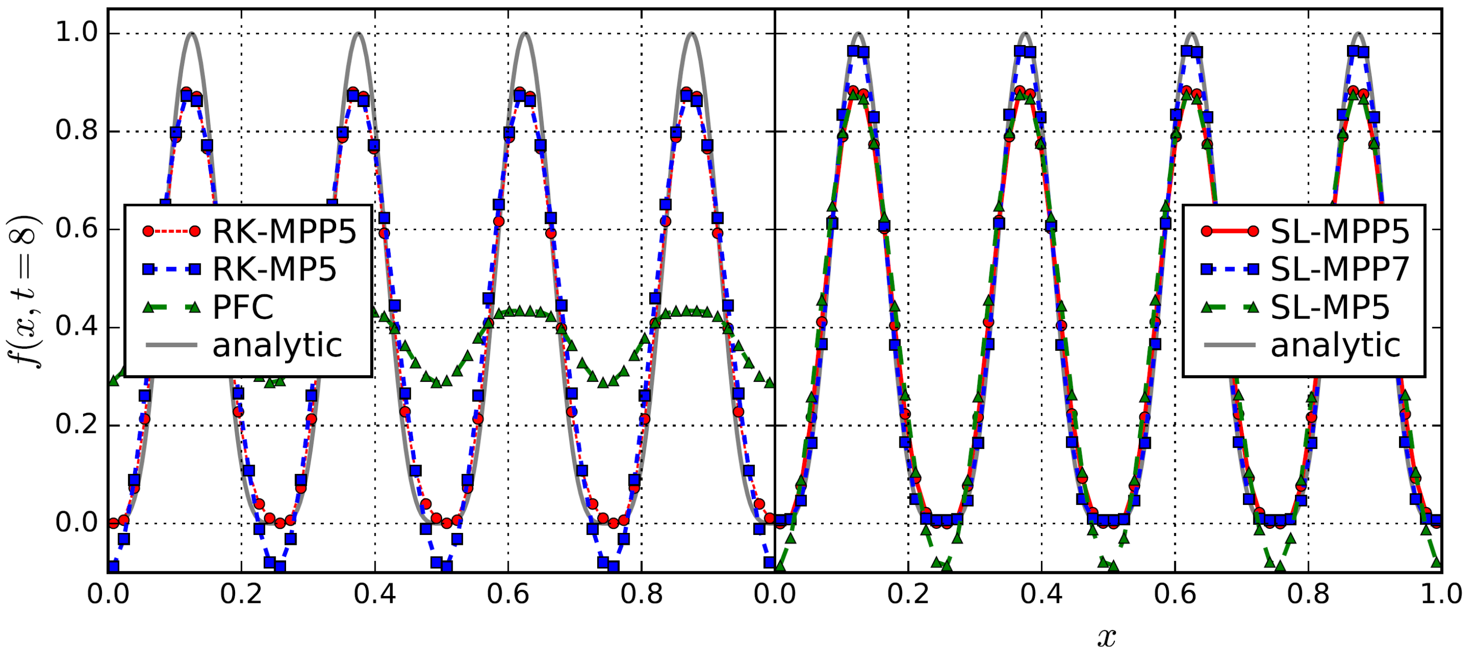

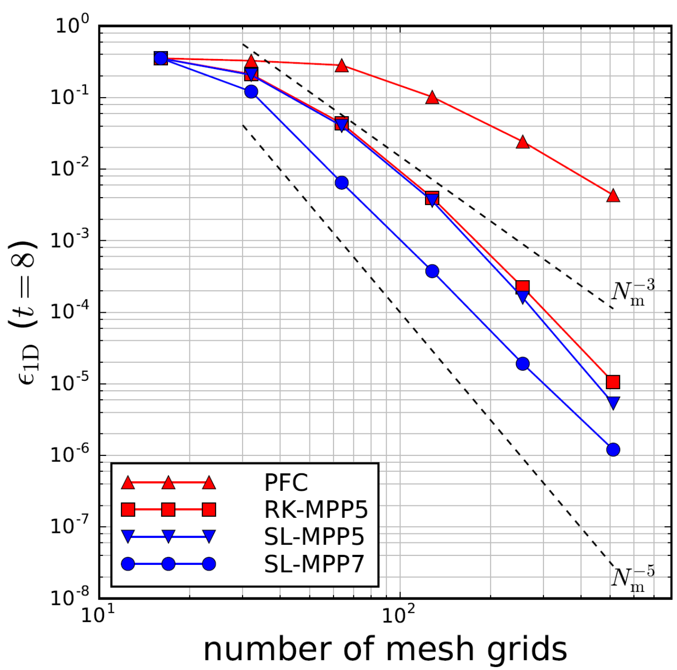

- The result of PFC scheme is severely smeared.
- Schemes w/o PP limiter yield significant negative value around the minima.
- 7th-order scheme (SL-MPP7) can reproduce the maxima.

1D Self-Gravitating System

- one-dimensional space with periodic boundary condition

- initial condition

$$f(x,v,t=0) = \frac{\bar{\rho}[1 + A\cos(kx)]}{(2\pi\sigma^2)^{1/2}} \exp\left(-\frac{v^2}{2\sigma^2}\right)$$

$$\rho(x,t=0) = \bar{\rho}[1 + A\cos(kx)]$$

- critical Jeans wave number

$$k_{\mathrm{J}} = \left(\frac{4\pi G\bar{\rho}}{\sigma^2}\right)^{1/2}$$

$$\begin{cases} k < k_{\mathrm{J}} & \Rightarrow \text{gravitational instability} \\ k > k_{\mathrm{J}} & \Rightarrow \text{collisionless damping} \end{cases}$$

1D Self-Gravitating System

$k/k_{\rm J} = 0.5 \quad A = 0.01 \quad N_x = N_v = 64$

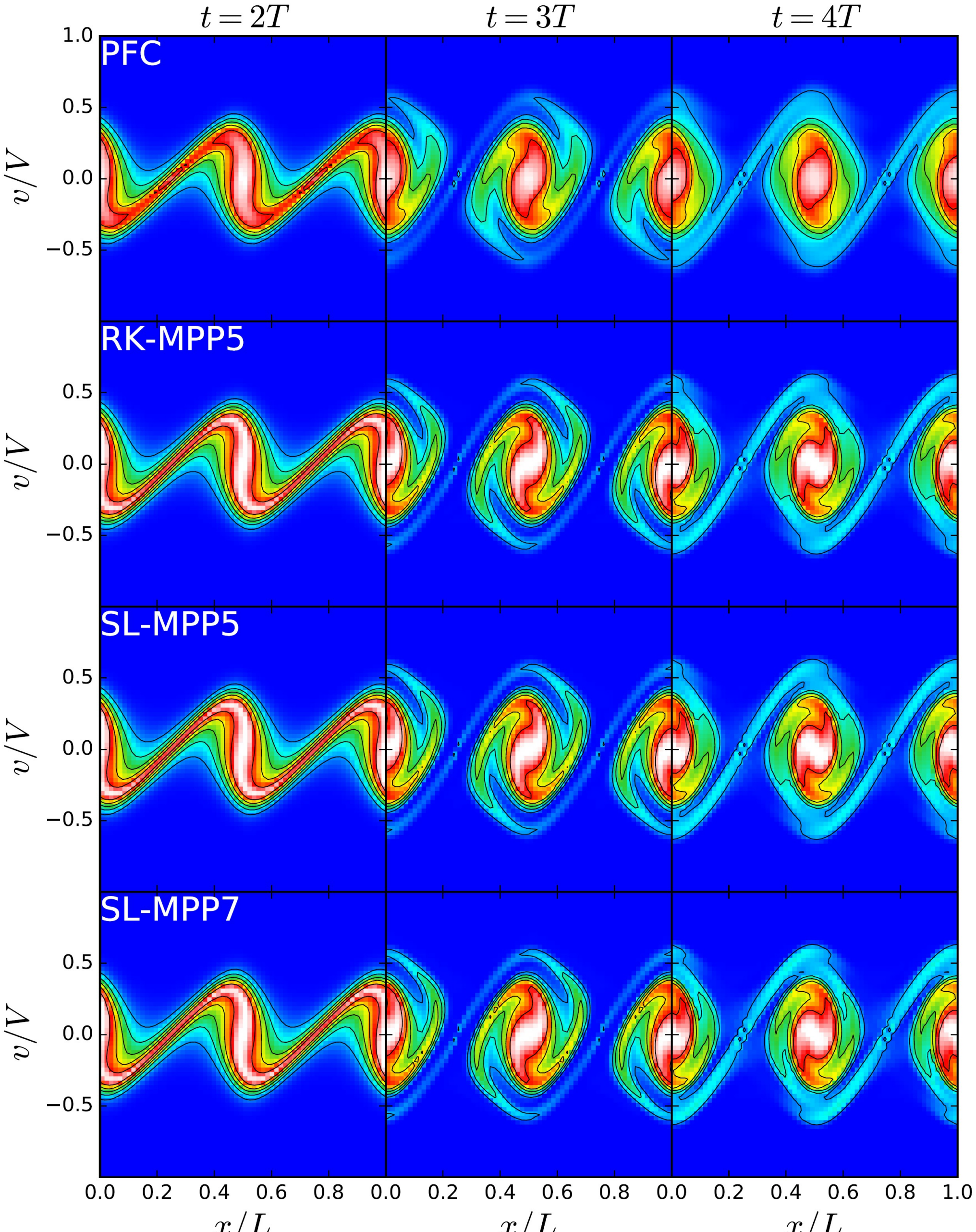

- As time proceeds, numerical diffusion takes place and smear small structures in the lower-order schemes.

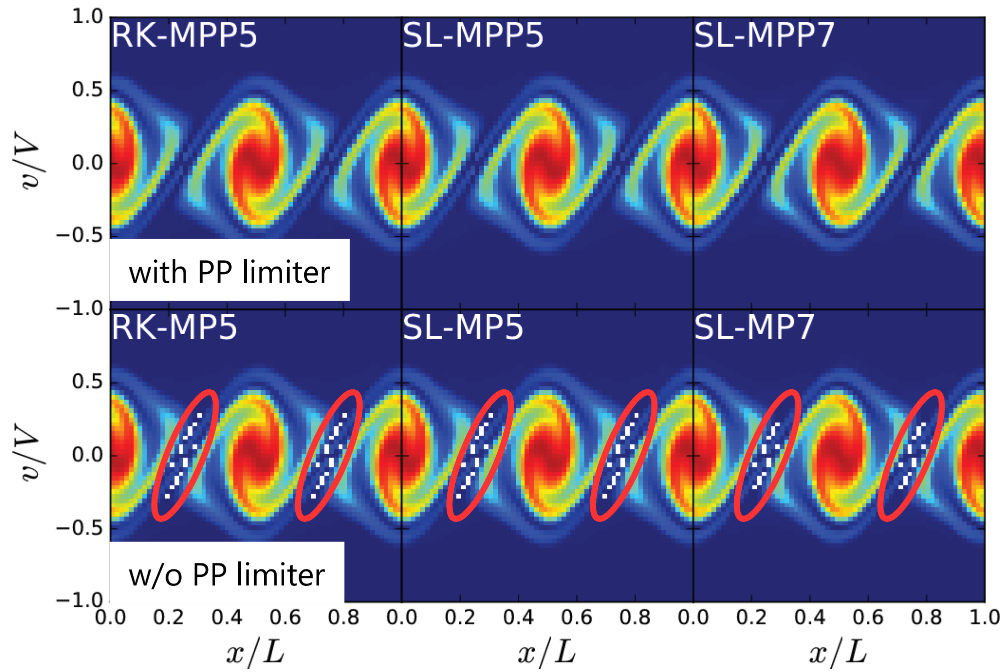

- Negative regions in the lower panels disappear in the results with positivity preserving limiter.

Application To Cosmological Neutrinos

Cosmological Relic Neutrinos

- massive neutrinos in the universe
  - lots of neutrinos in our universe decoupled at early stage of the universe when they are relativistic.
  - Discovery of neutrino oscillation

$$\sum m_\nu > 0.05 \text{ eV}$$

  - currently non-relativistic and gravitationally interacting with cold dark matter (CDM)
  - absolute mass of neutrinos and its hierarchy are still unknown

- dynamical effect of massive neutrinos

free streaming (collisionless damping)

  - large velocity dispersion of neutrinos $\sigma \sim 150(1+z)\left(\frac{m_\nu}{1\text{eV}}\right)^{-1} \text{km/s}$
  - growth of density fluctuation suppressed beyond the damping scale

$$k_{\rm FS} = \left(\frac{4\pi G\rho}{\sigma^2}\right)^{1/2} \Rightarrow \lambda_{\rm FS} \sim 640 \left(\frac{\Omega_{\rm m}}{0.3}\right)^{-1/2} \left(\frac{m_\nu}{1\text{eV}}\right)^{-1/2} h^{-1}\text{Mpc}$$

Collisionless Damping on LSS

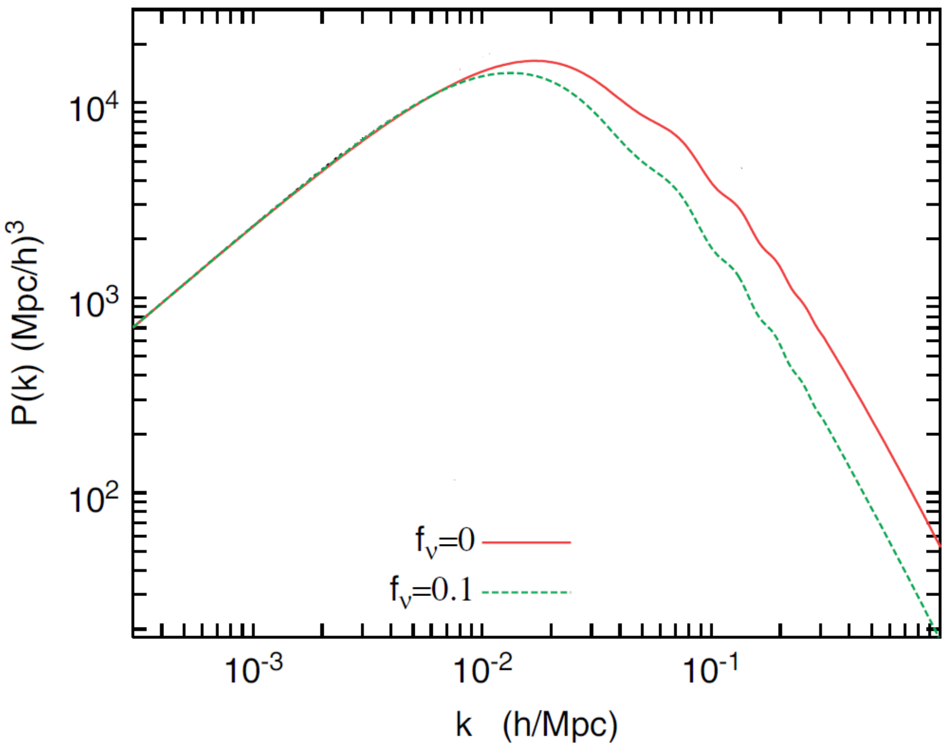

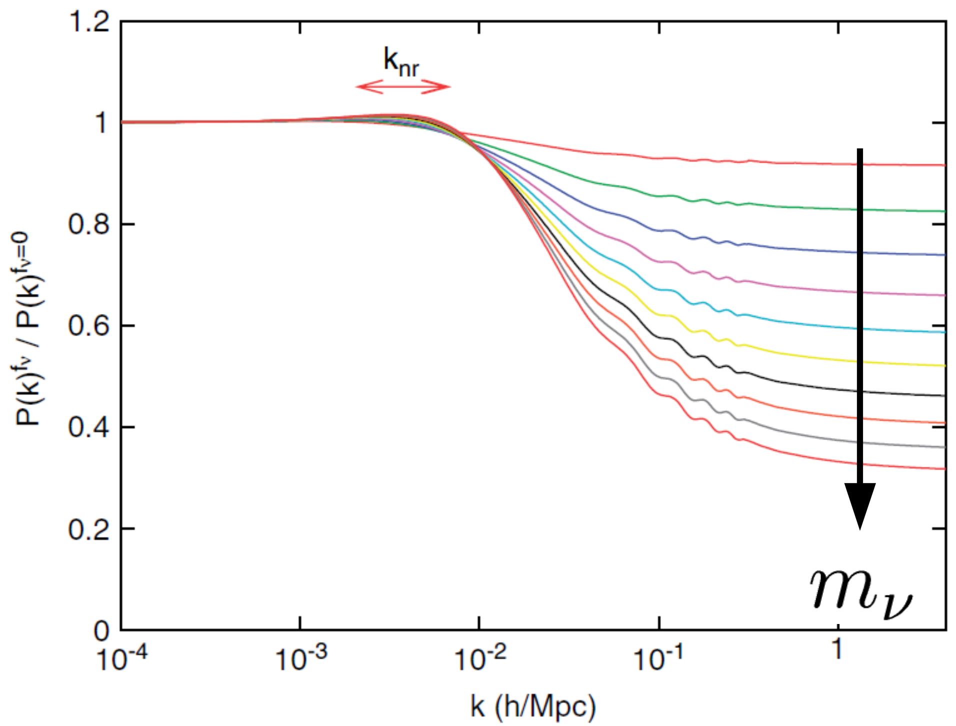

- density fluctuation suppressed at scales smaller than the damping scale.
- the amount of suppression depends on the mass of neutrinos
- the mass (and its hierarchy) of neutrinos can be estimated with such damping feature.
- non-linear features should be investigated with numerical simulations.

Hybrid of N-body and Vlasov Simulation

- Two-component (CDM and neutrino) simulation of the large-scale structure formation
- *N*-body method for CDM since it is "cold".
  - Equation of motion in the cosmological comoving coordinate

$$\frac{d^2\vec{x}_i}{dt^2} + 2H\frac{d\vec{x}_i}{dt} = -\frac{1}{a^2}\nabla\phi$$

- Vlasov simulation for neutrinos to follow its kinetic behavior and collisionless damping
  - Vlasov equation in the comoving coordinate

$$\frac{\partial f}{\partial t} + \frac{\vec{v}}{a}\cdot\frac{\partial f}{\partial \vec{x}} - \left[H\vec{v} + \frac{\nabla\phi}{a}\right]\cdot\frac{\partial f}{\partial \vec{v}} = 0$$

- Poisson equation computes the gravitational potential contributed by both of CDM and nuetrinos.

$$\nabla^2\phi = 4\pi G\bar{\rho}a^2(f_{\rm cdm}\delta_{\rm cdm} + f_\nu\delta_\nu)$$

Initial Condition

- cosmological parameters

  PLANCK 2015 results : $\Omega_{\rm m} = 0.308,\ \Omega_\Lambda = 0.692,\ \Omega_{\rm b} = 0.0484,\ h = 0.678$

  curvature fluctuation : $A_{\rm s} = 2.3723 \times 10^{-9}$ (pivot scale : k = 0.002 Mpc^{-1})

- total neutrino mass

$$\sum_i m_i = 0.4\ \mathrm{eV}\ \ (\Omega_\nu = 0.0043h^{-2})$$

- initial condition created at redshift of $z_{\rm i}$ = 10

- computaional domain: $L_{\rm box}$ = 20000h^{-1} Mpc, 2000h^{-1} Mpc, 200h^{-1} Mpc

- number of particles / number of mesh grids

  N-body simulation : $N_{\rm p} = 1024^3$

  Vlasov simulation : $N_{\rm x} = 128^3, N_{\rm v} = 32^3$

CDM and neutrino distribution

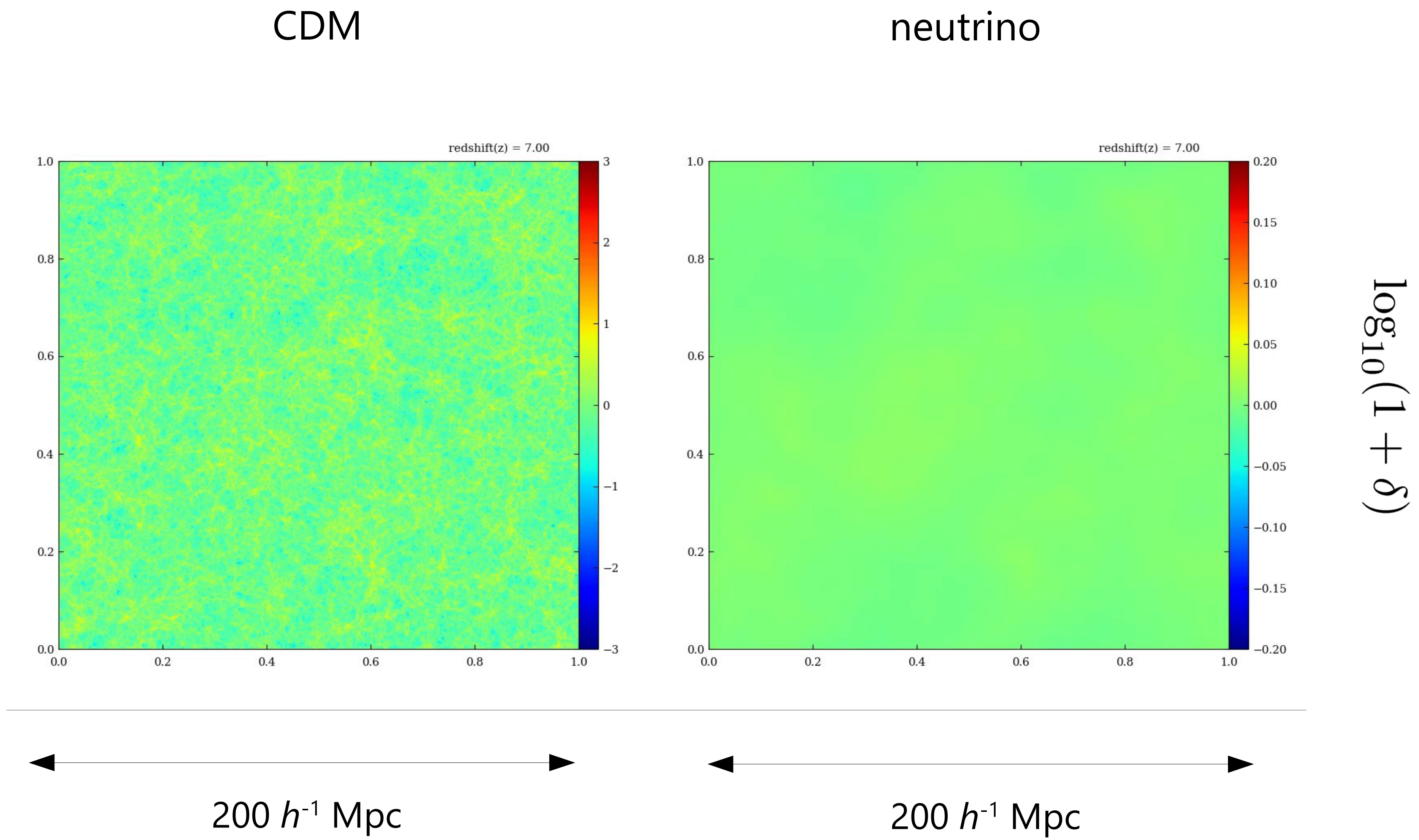

Power Spectrum

$$\frac{P(k, f_\nu)}{P(k, f_\nu = 0)}$$: ratio of power spectra with massive and massless neutrinos

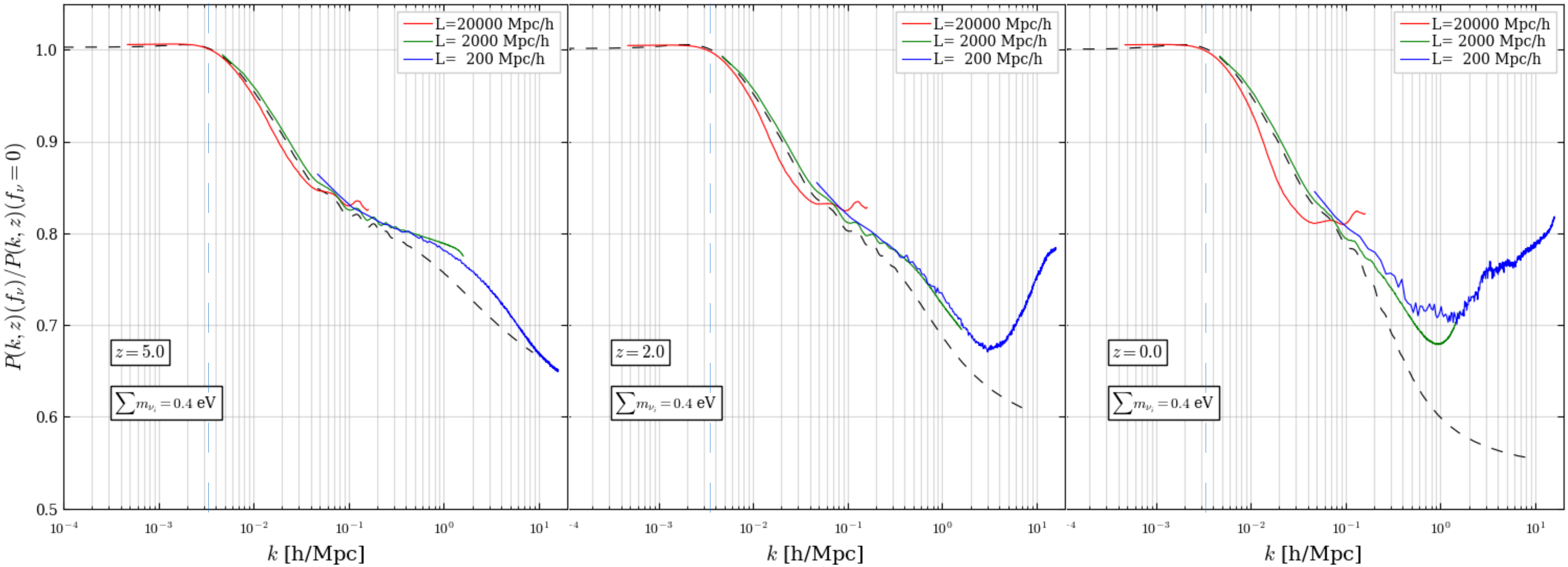

damping scale : $k_{\rm nr} = \sqrt{\dfrac{4\pi G\bar{\rho}(t_{\rm nr})a(t_{\rm nr})^2}{\sigma_\nu^2(t_{\rm nr})}} \simeq 0.018\Omega_{\rm m}^{1/2}\left(\dfrac{m}{1\,{\rm eV}}\right)^{1/2} h\ {\rm Mpc}^{-1} = 3.5\times10^{-3} h\,{\rm Mpc}^{-1}$

- density fluctuation with k > 3x10^{-2} h/Mpc damps owing to collisionless damping
- consistent with the perturbation theory (e.g. Saito et al. 2009) in the early stages
- up turn at k>1 h^{-1}Mpc, probably due to dynamical feedback by CDM

CDM and neutrino distribution

contour : CDM　　　　　color : neutrino

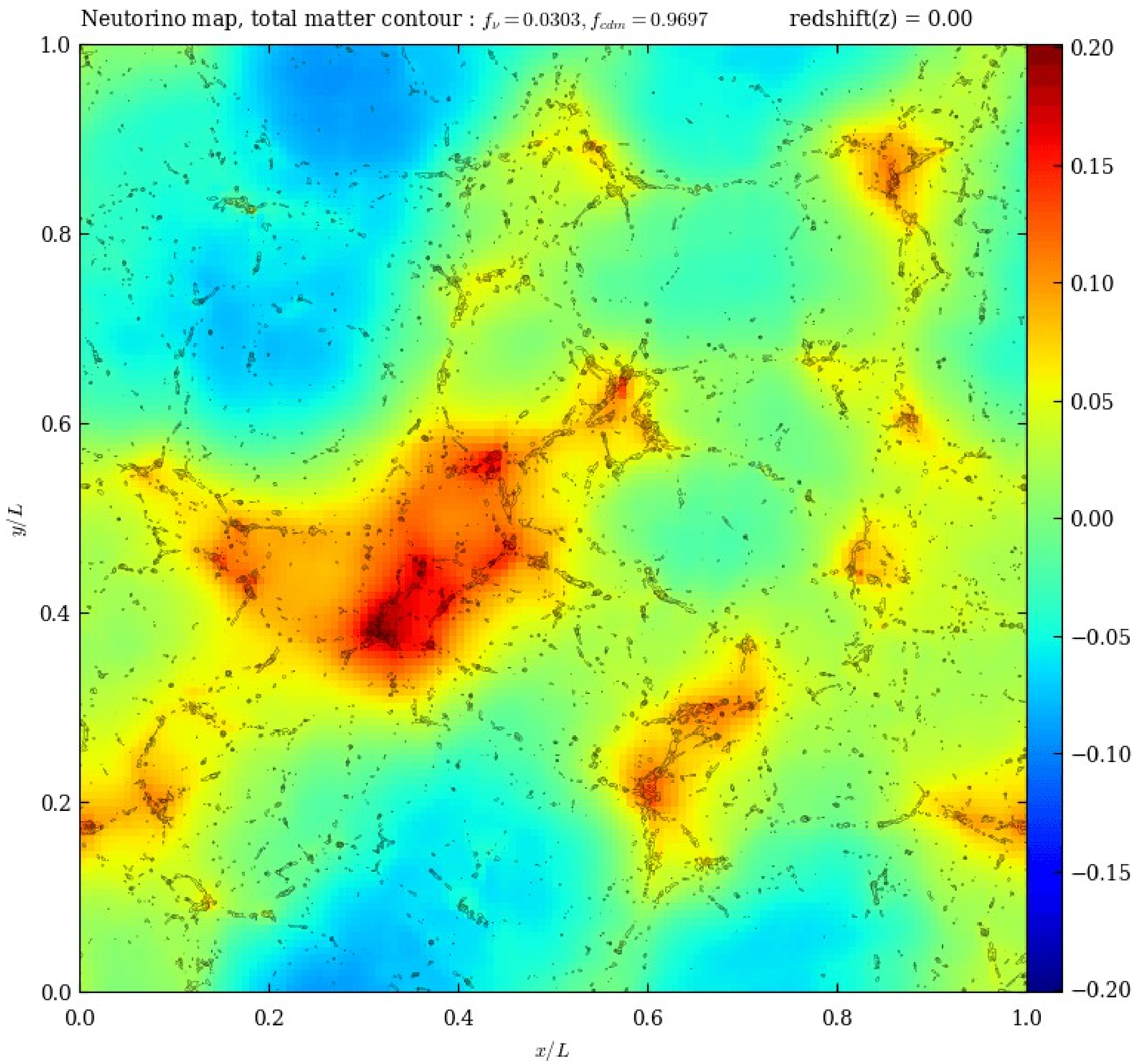

200 h^{-1} Mpc

- diffuse distribution of neutrinos owing to its large velocity dispersion
- regions with similar CDM density can have significantly different neutrino density
- remarkable offset in density peaks of CDM and neutrinos

neutrino wake / dynamical friction ?

Zhu et al. (2016)

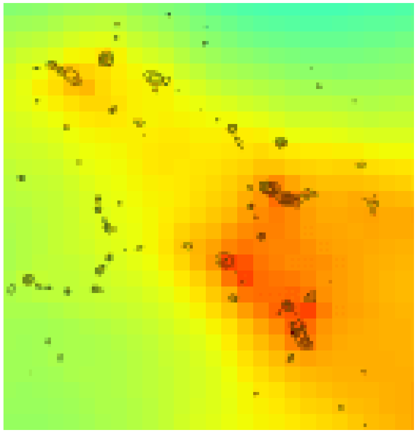

40 h^{-1} Mpc

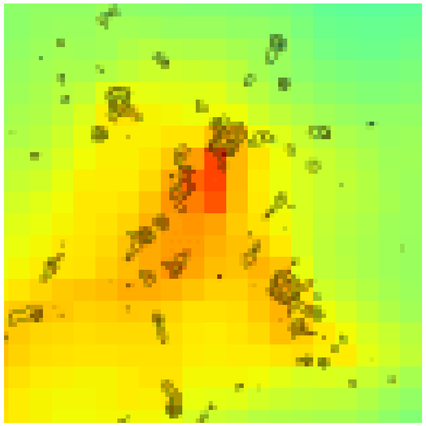

20 h^{-1} Mpc

Vlasov-Maxwell Simulation

Vlasov-Maxwell Simulation

$$\frac{\partial f_s}{\partial t} + \boldsymbol{v} \cdot \frac{\partial f_s}{\partial \boldsymbol{x}} + \frac{q_s}{m_s}\left(\boldsymbol{E} + \boxed{\frac{\boldsymbol{v} \times \boldsymbol{B}}{c}}\right) \cdot \frac{\partial f_s}{\partial \boldsymbol{v}} = 0$$

$$\frac{\partial \boldsymbol{E}}{\partial t} = c\nabla \times \boldsymbol{B} - 4\pi \boldsymbol{J}$$

$$\boldsymbol{J} = \sum_s \int q_s \boldsymbol{v} f_s \mathrm{d}^3 \boldsymbol{v}$$

$$\frac{\partial \boldsymbol{B}}{\partial t} = -c\nabla \times \boldsymbol{E}$$

- solve the distribution functions for both of ions and electrons
- difficulty to solve gyro-motion in the velocity space corrrectly correctly in the long term
- rigid-body rotation problem

$$\frac{\partial f}{\partial t} + (\boldsymbol{r} \times \boldsymbol{\omega}) \cdot \frac{\partial f}{\partial \boldsymbol{r}} = 0$$

rigid-body rotation of a 2D gaussian profile

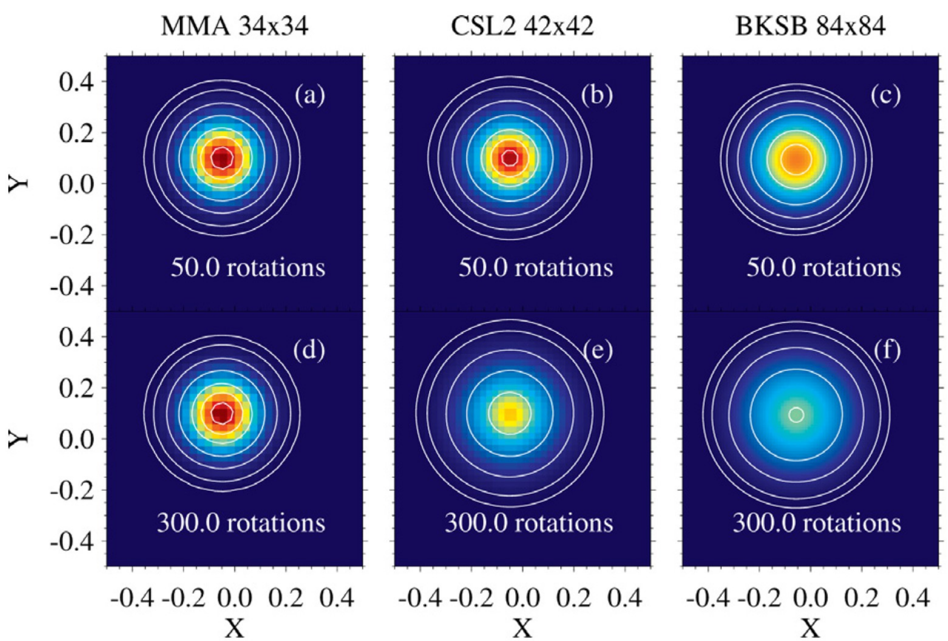

Minoshima, Matsumoto, Amano (2011)

temporal variation of dispersion

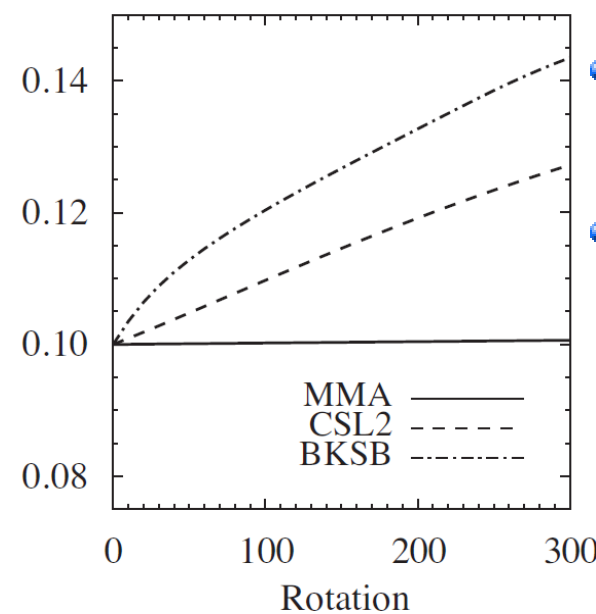

- CSL2 : CIP-CSL2

  Takizawa et al. (2002)
- BKSB : backsubstitution method

  Schmitz & Grauer (2006)

Rigid-Body Rotation with Our Scheme

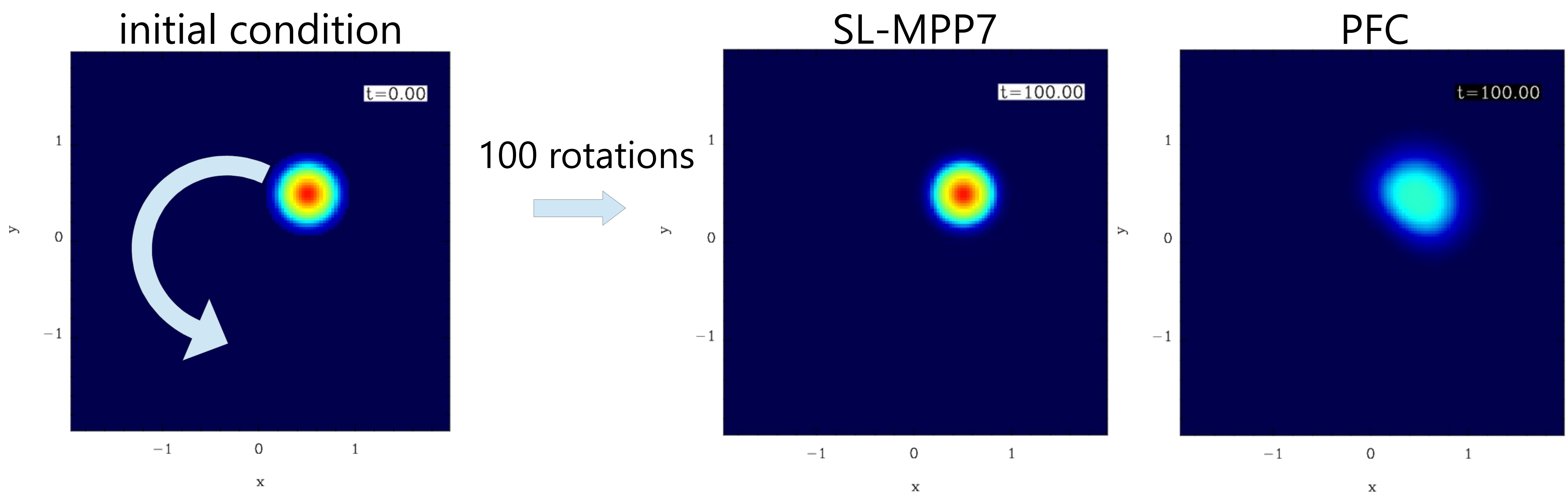

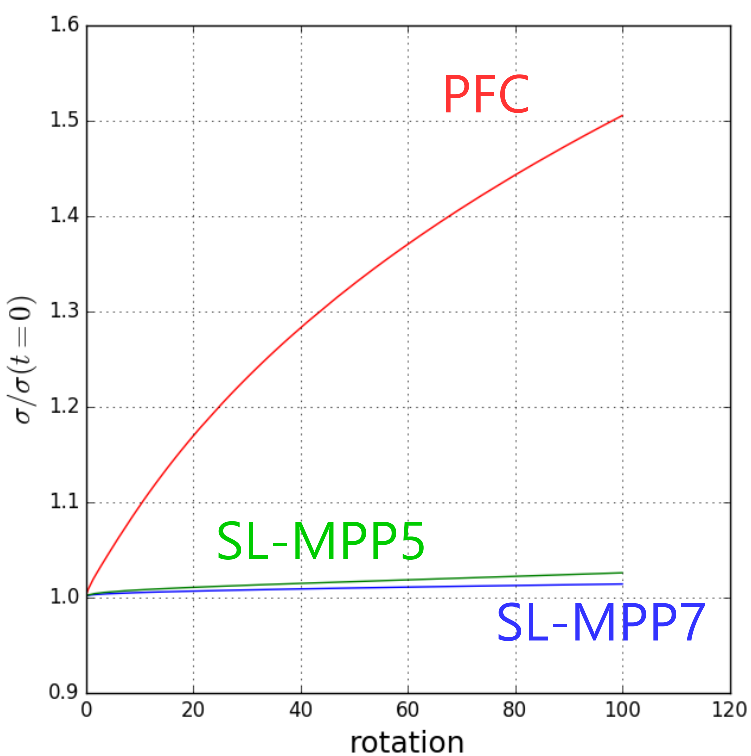

- rigid-body rotation of a gaussian profile in a 2D plane
- SL-MPP5 and SL-MPP7 schemes yields only a few per cent increase in velocity dispersion.
- The lower-order scheme suffers from significant numerical heating.

Magnetic Reconnection

- Vlasov-Maxwell simulation in 5D phase space
  - N_x=432, N_y = 216
  - $N_{vx} = N_{vy} = N_{vz} = 32$
  - Hall effect to trigger the fast reconnection

color : $\boldsymbol{J}_z$

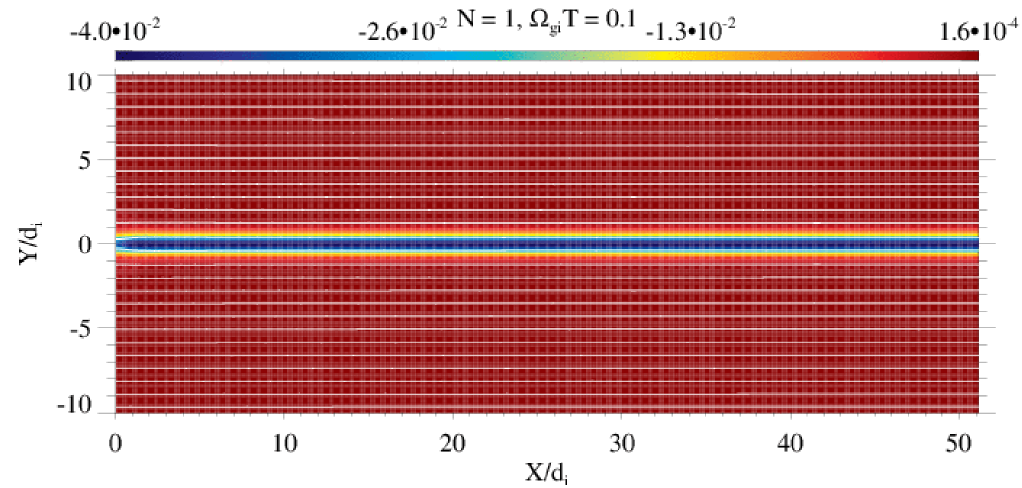

$$\boldsymbol{J} \cdot \left(\boldsymbol{E} + \frac{\boldsymbol{v} \times \boldsymbol{B}}{c} \right)$$

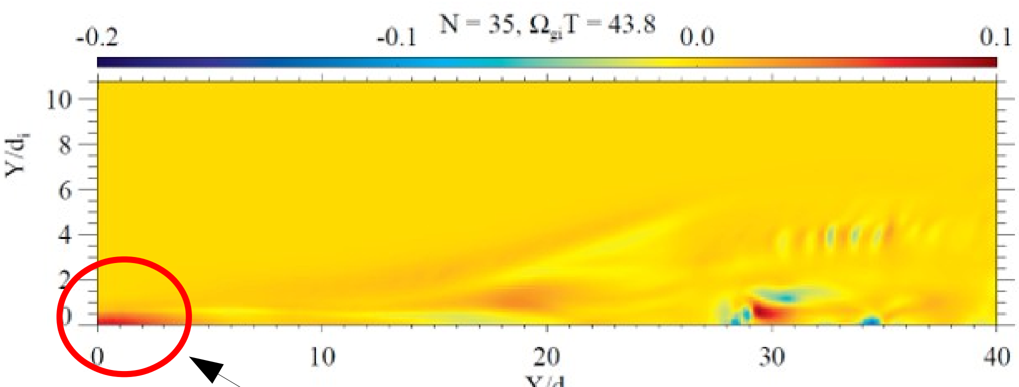

dissipation of magnetic field

$$\frac{\partial \rho v_x}{\partial t} + \nabla \cdot (\rho v_x \boldsymbol{v}) + \frac{\partial p}{\partial x} + \frac{q \rho v_z B_y}{mc}$$

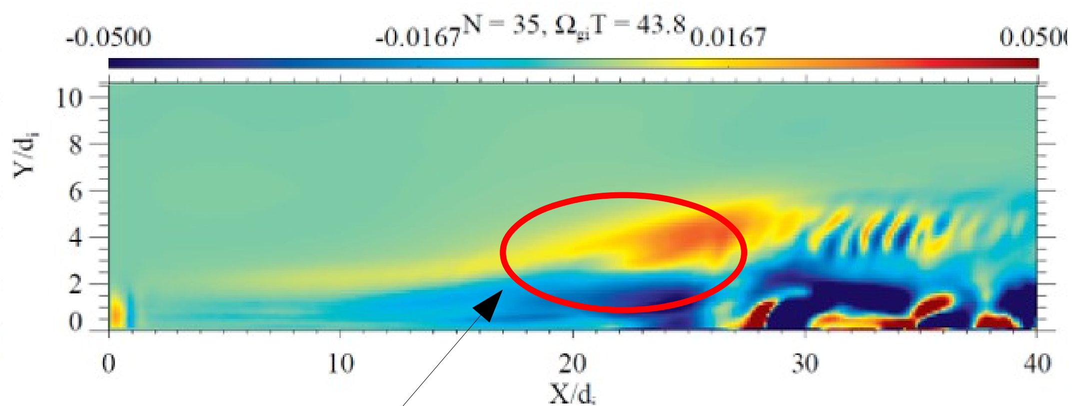

momentum transport to upstream region

Magnetic Reconnection

- Vlasov-Maxwell simulation in 5D phase space
  - N_x=432, N_y = 216
  - $N_{vx} = N_{vy} = N_{vz} = 32$
  - Hall effect to trigger the fast reconnection

color : $\boldsymbol{J}_z$

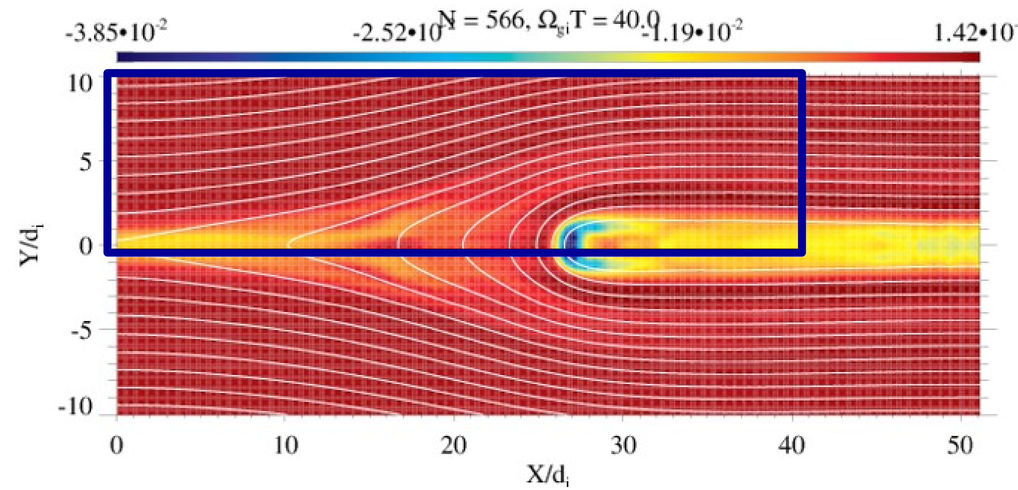

$$\boldsymbol{J} \cdot \left(\boldsymbol{E} + \frac{\boldsymbol{v} \times \boldsymbol{B}}{c} \right)$$

$$\frac{\partial \rho v_x}{\partial t} + \nabla \cdot (\rho v_x \boldsymbol{v}) + \frac{\partial p}{\partial x} + \frac{q \rho v_z B_y}{mc}$$

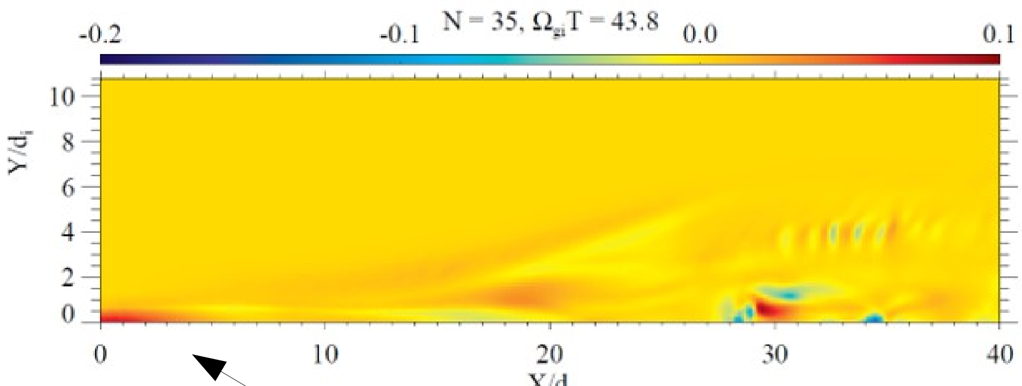

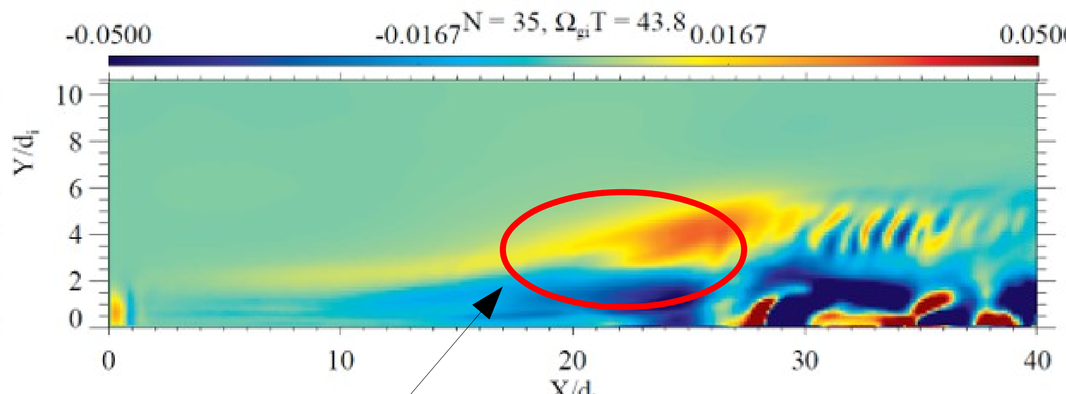

dissipation of magnetic field

momentum transport to upstream region

Summary

- Vlasov simulations in 6-dimensional phase space are now practical.
- A new high-order advection scheme with monotonicity- and positivity-preservation and with single-stage time integration
- Vlasov-Poisson simulation of cosmic neutrinos in the large-scale structure in the universe

Neutrino Mass

- Findings of the neutrino oscillation

$m_1 \quad m_2 \quad m_3$: masses of three eigen states

$$m_2^2 - m_1^2 = 7.9^{+1.0}_{-0.8} \times 10^{-5}\ \mathrm{eV}$$

$$|m_3^2 - m_1^2| = 2.2^{+1.1}_{-0.8} \times 10^{-3}\ \mathrm{eV}$$

$$\sin^2\theta_{12} = 0.3^{+0.10}_{-0.06}$$

$$\sin^2\theta_{23} = 0.5^{+0.18}_{-0.16}$$

$$\sin^2\theta_{13} < 0.043$$

Lesgourgues & Pastor (2006)

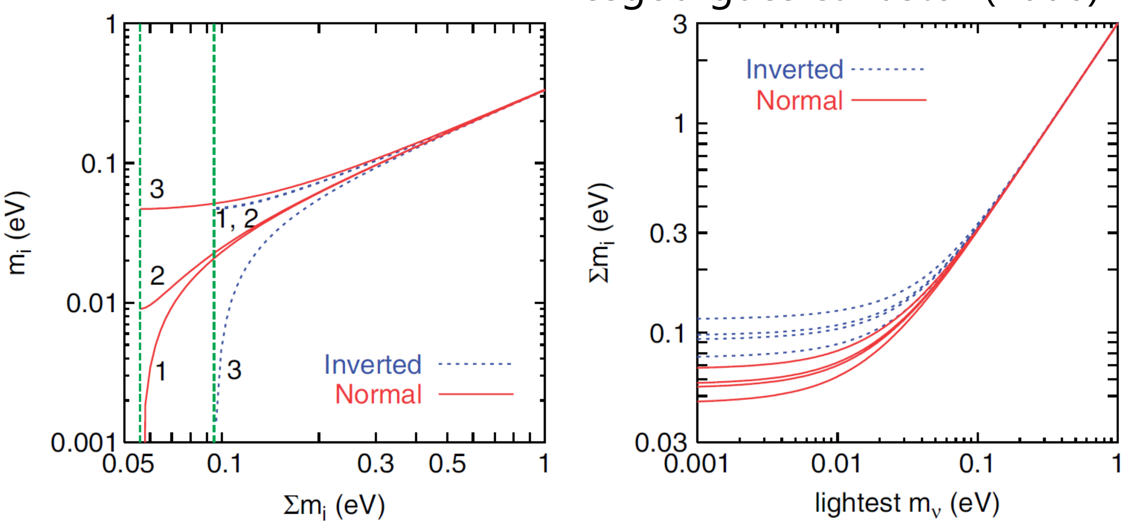

- mass hierarchy

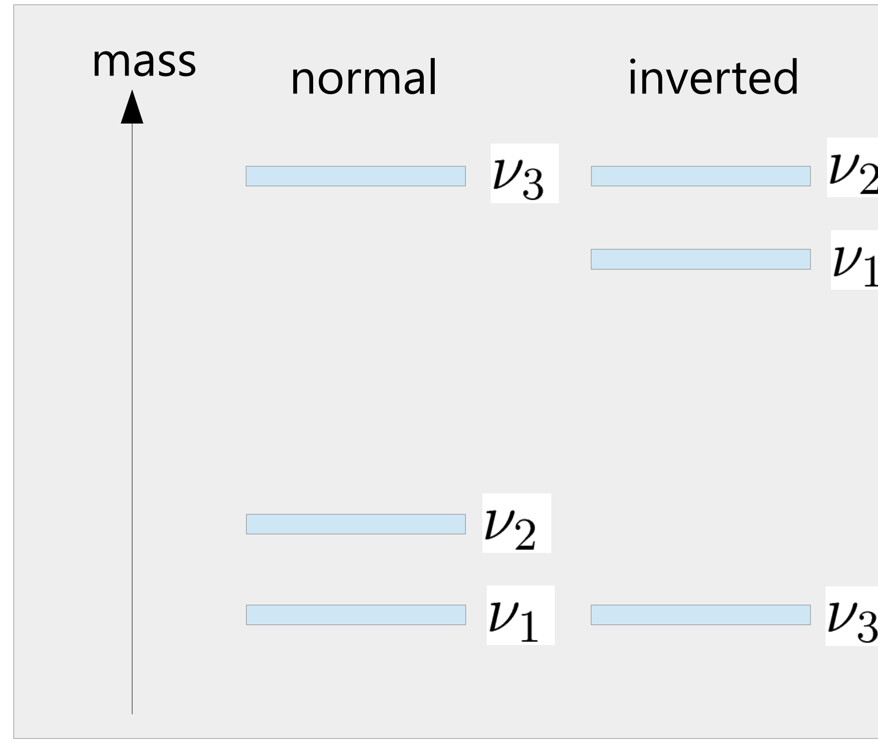

- Constraints on total neutrino mass

$$0.05\,\mathrm{eV} \le \sum_i m_i \le 6\,\mathrm{eV}$$

constraints of tritium beta decay

Cosmological Relic Neutrino

- thermal history of cosmological neutrinos

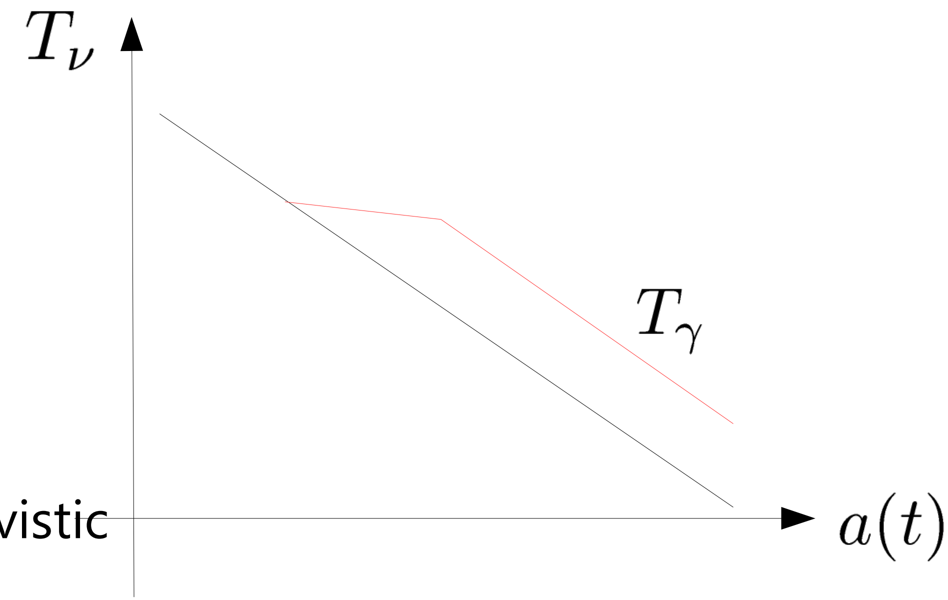

heating of photons by electron-positron annhilation

$$T_\gamma = \left(\frac{11}{4}\right)^{1/3} T_\nu$$

- epoch when neutrinos become non-relativistic

$$1 + z_{\rm nr} = 1890 \left(\frac{m_i}{1\,{\rm eV}}\right)$$

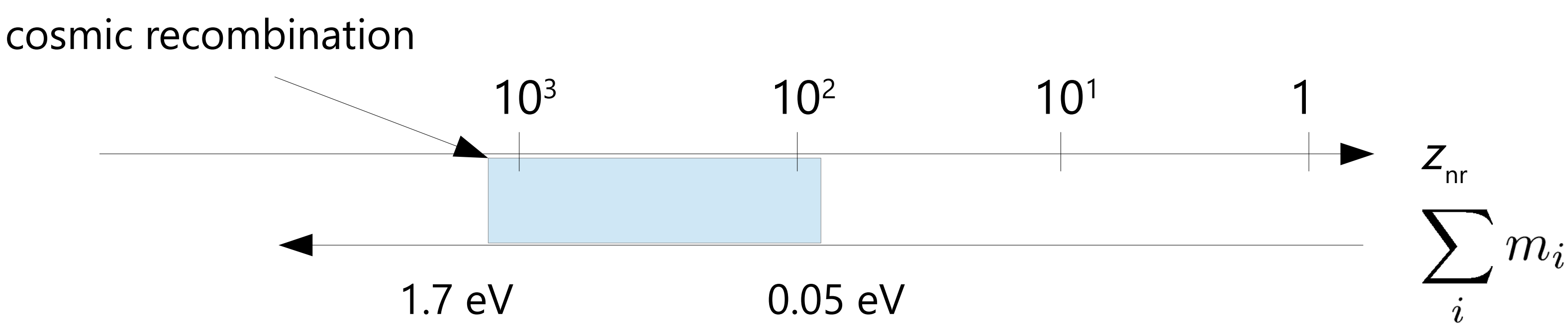

- upper bound of total neutrino mass based on the Plack result 2015

Planck collaboration 2015

Parameter	TT	TT+lensing	TT+lensing+ext	TT, TE, EE	TT, TE, EE+lensing	TT, TE, EE+lensing+ext
Σm_ν [eV]	< 0.715	< 0.675	< 0.234	< 0.492	< 0.589	< 0.194

Cosmological Formulation of Vlasov-Poisson Equations

- Vlasov-Poisson equation in canonical variables

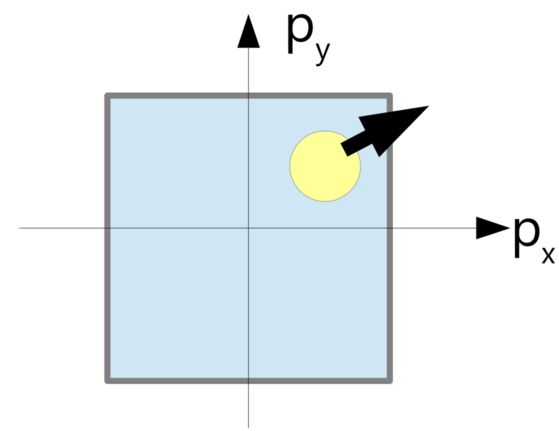

$$\frac{\partial f}{\partial t} + \frac{\vec{p}}{a^2} \cdot \frac{\partial f}{\partial \vec{x}} - \nabla \phi \cdot \frac{\partial f}{\partial \vec{p}} = 0 \qquad \vec{p} = a^2 \dot{\vec{x}}$$

$$\nabla^2 \phi = 4\pi G a^2 \bar{\rho} \delta = 4\pi G a^2 \bar{\rho} \left[\int f d^3 \vec{p} - 1 \right]$$

  - Velocity extent exceeds the computational velocity domain as the universe expands

- Formulation suitable to Vlasov-Poisson simulations in cosmological coordinate.

$$\frac{\partial f}{\partial t} + \frac{\vec{v}}{a} \cdot \frac{\partial f}{\partial \vec{x}} - \left[H\vec{v} + \frac{\nabla \phi}{a} \right] \cdot \frac{\partial f}{\partial \vec{v}} = 0$$

- peculiar velocity $v = a\dot{x}$ instead of canonical momentum.
- advection "velocity" in the velocity space depends on the "position" in the velocity space

Vlasov-Poisson Simulation of the Large-Scale Structure Formation